



HAL
open science

Surface charges effects on the 2D conformation of supercoiled DNA

Tatiana Schmatko, Pierre Muller, Mounir Maaloum

► **To cite this version:**

Tatiana Schmatko, Pierre Muller, Mounir Maaloum. Surface charges effects on the 2D conformation of supercoiled DNA. *Soft Matter*, 2014, pp.2469-2704. hal-00696100v2

HAL Id: hal-00696100

<https://hal.science/hal-00696100v2>

Submitted on 11 Dec 2014

HAL is a multi-disciplinary open access archive for the deposit and dissemination of scientific research documents, whether they are published or not. The documents may come from teaching and research institutions in France or abroad, or from public or private research centers.

L'archive ouverte pluridisciplinaire **HAL**, est destinée au dépôt et à la diffusion de documents scientifiques de niveau recherche, publiés ou non, émanant des établissements d'enseignement et de recherche français ou étrangers, des laboratoires publics ou privés.

ARTICLE

Surface charges effects on the 2D conformation of supercoiled DNA

Cite this: *Soft Matter*, 2014, 10, 2520Tatiana Schmatko^{a*}, Pierre Muller^a and Mounir Maaloum^a,Received 10th December 2013,
Accepted 10th January 2014

DOI: 10.1039/c3sm53071j

www.rsc.org/

We have adsorbed plasmid pUc19 DNA on a supported bilayer. By varying the fraction of cationic lipids in the membrane, we have tuned the surface charge. Plasmid conformations were imaged by Atomic Force Microscopy (AFM). We performed two sets of experiments: deposition from salt free solution on charged bilayers and deposition from salty solutions on neutral bilayers. Both sets show similar trends: at low surface charge density or low bulk salt concentration, internal electrostatic repulsion forces plasmids to adopt completely opened structures, while at high surface charge density or higher bulk salt concentration, usual supercoiled plectonemes are observed. We experimentally demonstrate the equivalence of surface screening by mobile interfacial charges and bulk screening from salt ions. At low to medium screening, the electrostatic repulsion at plasmid crossings is predominant, leading to a number of crossovers decreasing linearly with the characteristic screening length. We compare our data with an analytical 2D-equilibrated model developed recently for the system and extract the DNA effective charge density when strands are adsorbed at the surface.

Introduction

Since its discovery¹, supercoiled DNA has been extensively studied by biologists and by physicists. The former were mostly interested in its implication in biological processes²⁻⁸, the later were amazed by the beauty of its structure and studied its topology and conformation^{9, 10}. Topology and conformation are inter-dependent so that, in order to study the conformation of a supercoiled DNA we need to define a few topological concepts.

In nature, enzymes promote winding of one strand around the other during many cell processes, this is what causes supercoiling. In fact, supercoiled DNA is made of closed circular double stranded DNA where one strand usually winds around the other a specific number of times. As long as the two circular strands are not broken, this number is fixed; it is called the linking number L_k . The helical nature of double-stranded

DNA leads as well to some natural twist. There is an intrinsic linking number Lk_0 corresponding to the unconstrained number of helical turns for a DNA of a specific length. However the linking number Lk is generally not equal to Lk_0 , it is usually a little smaller. Therefore one introduces the difference: $\Delta Lk = Lk - Lk_0$. As Lk_0 increases with the DNA length, in practice one uses the supercoiled density σ , which as an intensive parameter, enables the comparison of plasmids of different lengths:

$$\sigma = \frac{\Delta Lk}{Lk_0}$$

Two other numbers are of great importance: the Twist number T_w and the Writhing number W_r . These three quantities are linked by the following equation: $L_k = T_w + W_r$. For a fixed linking number, twist can be traded against writhe. A supercoiled DNA molecule attempts to relax its torsional stress by writhing. Segments of the chain go successively above and below others which finally defines the tertiary structure of the molecule. Writhe gives rise to extra bending. The conformation is fixed by a balance between twist and bending energies in physiological conditions. At lower salt concentrations, the electrostatic repulsion between strands is also involved. For DNA in solution, it is possible to adopt, non-planar conformations, with the lowest total energy that leads to some torsional twist. The reduction of the torsional energy is accompanied by an increase of the bending energy.

^a Institut Charles Sadron, CNRS UPR 22 et Université de Strasbourg, 23 rue du loess BP 84047 67034 Strasbourg Cedex2, France.

* To whom correspondence should be addressed: E-mail: tatiana.schmatko@ics-cnrs.unistra.fr

† Electronic Supplementary Information (ESI) available: [Fig S1: Langmuir Blodgett Isotherms for DPPC/DPTAP mixed monolayers, Fig S2: Isopressures measurements of the area per lipid head for mixed DDPC/DPTAP monolayers, as a function of the charge fraction, Fig S3: Evolution of the DNA absorbance at 260 nm as a function of time and temperature]. See DOI: 10.1039/b000000x/

There is an additional electrostatic energy contribution, which favours slightly open structures. The equilibrium shape thus also depends on the salt concentration in solution. For non-planar geometries, the torsional energy is proportional to $(Tw - Lk_0)^2$, therefore, in practice, Tw remains close to Lk_0 , by adopting a conformation with Wr close to ΔL_k . For a planar closed double helix, without any writhe, the constraint of ΔL_k would give rise to a huge torsional energy, proportional to ΔL_k^2 .

Much is known about the conformation of supercoiled DNA in solution, mostly under the physiological conditions relevant in biology. Many experiments using gradient centrifugation¹¹ and electrophoresis have been performed in the late 70's. They tend to give precise values for W_r , T_w and σ , as well as ratios between them^{12, 13}. The first electron microscopy (EM) images of plasmids were available roughly ten years later^{10, 14-17}. This was the first time one could see what supercoiled DNA looks like. In these experiments, supercoiled DNA is shown to have a plectonemic conformation. For very long DNAs, these plectonemes may have branches as well. It is described as a superhelix of radius r . The number of crossings of one strand above or below the other is n . $W_r = n \cdot \sin \alpha$, where α is the angle between the tangent to one helix and the plane perpendicular to the superhelix axis. One of the works of reference is by Boles et al¹⁰. It shows perfectly regular plectonemes with a particularly well defined superhelix radius. In this study the authors precisely measured n , r and α and compared their results with those obtained from solution measurements. These observations were confirmed by molecular simulations¹⁸⁻²⁴. AFM data arrived later²⁵⁻³⁵. They systematically show loosely interwound conformations. The observed conformations are much less regular than those seen in EM. Small variations were observed from experiments to experiments, and sometimes the results were discarded because they did not show plectonemic conformations. In 2002 Zhakharaeva et al³⁶ performed small angle neutron scattering on supercoiled DNA. Their results are in agreement with pioneering EM work. For instance, they obtained in 50 mM NaCl an opening angle α of 50° and a superhelix radius r of 10nm. Surprisingly the superhelix radius distribution was rather large (± 4 nm) in comparison with EM measurements. This cannot be attributed to the precision of the measurement as the resolution of neutron scattering is much better than 4 nm. These results could then go in favour of the AFM loose conformations as well. Neutron scattering does not perturb the molecule and can be trustfully considered, but it is rather difficult to transpose the results to real space. On the other hand, real space experiments like AFM and TEM require the deposition of the molecule at the surface, whose effect on the conformation is often underestimated. Actually it is an important issue. One might think that the problem of surface effects was solved with the appearance of cryo-EM which is surely a real improvement in this direction^{7, 37}. With cryo-EM, the sample solution is frozen and micro sliced before imaging, such as we may think that the observed conformation is the real

3D conformation. The results obtained with cryo-EM were by many aspects comparable to those from pioneering TEM work. For example the idea of a perfectly regular 3D, plectonemic conformation was reinforced. Nonetheless, cryo-EM can generate surface artefacts as well. Sample preparation is very subtle and small volumes are required. The sample thickness is often of the same order of magnitude as size of the molecule, confinement may occur before freezing at the air/water interface which will modify the structure and arrangements of the molecules³⁷. At large ionic strength, cryo-EM also showed strong deviations from solution measurements; unexpectedly, the gyration radius of the molecule was seen to increase with the salt concentration^{14, 17}. This discrepancy was attributed to a quenching of the conformation at very low temperature. Indeed, the native twist of the DNA molecule should increase when the temperature is decreased. Simulations at -50°C have confirmed this assumption³⁸.

Our goal in this article is to understand the influence of surface charges when supercoiled DNA is confined in 2D, and to help rationalize seemingly conflicting observations reported in the literature. The physics of the problem is complex. There is entropy loss consecutive to DNA adsorption, entropy gain consecutive to counter-ions release, and there are various electrostatic interactions. For constrained cyclic DNA, supercoiling introduces an extra level of complexity. All these aspects enter the description with an impact depending on the concentration of salt in solution. Vologodski and Cozzarelli³⁹ performed simulations in order to elucidate the influence of the surface on the conformation of supercoiled DNA. This work focused on non-equilibrium immobilization. Later on, Velichko and coworkers⁴⁰ did molecular simulations on supercoiled semi flexible polymers and reported writhe gain when the macromolecule was adsorbed on a surface. The model used to describe the supercoiled macromolecule was a freely-joined chain with uncharged segments. Their study was dedicated to the entropic and mechanical deformation aspects then their conclusions apply probably well to DNA at high salt concentrations. In a more recent Monte Carlo simulation, Fujimoto and Schurr⁴¹ used a model previously validated with supercoiled DNA in solution. They added a surface potential to mimic the 2D immobilization of the molecule. Our own experiments will turn out to be quite close to their simulation results at equilibrium. The authors compared their computation with the AFM results from Lyubchenko and Shlyakhtenko²⁹ even though neither the surface charge of the amino-modified mica, nor the plasmid supercoiled density, were known. Their results match the AFM data at 160 mM salt and show that after surface immobilization, the DNA molecule seems to rearrange as an unbranched plectoneme. At 10 mM however, they show plectonemic conformations, while experiments were reporting quite open conformations, with multiple strands crossing nearly at the same point. The authors suggested that the unusual multi-arm conformations reported in AFM might be due to irregularities of the surface used for DNA fixing, or local

higher charge densities. Starting from this statement, Bussiek and Langowsky³³ performed AFM experiments where the DNA was deposited on polylysine films. The polymer density was varied. Testing linear DNA with the model from Rivetti et al⁴² on their surfaces, they showed that for high polylysine densities, DNA was immediately stuck and remained in a conformation that is a projection of the full 3D conformation. For plasmids of the same length they observed conformations that were irregular and frozen. For low polylysine densities, the linear DNAs reached an equilibrated 2D conformation and plasmids were observed with plectonemic conformations. They concluded that the plectonemes were the result of a 2D equilibrium conformation and that open or multi-arm or many crossing conformations were the result of a 3D freezing. This work is a good starting point toward the understanding of surface induced conformations, although internal polymeric electrostatics is not taken into account and surface charges were only considered as an adhesion promoter.

In the present article we present AFM experiments performed on surfaces with known surface charge densities. By adsorbing DNA on lipid bilayers whose composition was a mixture of cationic lipids and zwitterionic phospholipids, we have varied the surface charge quantitatively. Furthermore, lipids are mobile within a membrane which ensures that DNA molecules are not frozen and conformations should be equilibrated in 2D. The lipids diffusion coefficient has been measured by Fluorescence Recovery After Patterned Photobleaching (FRAPP)⁴³; it is $0.7 \mu\text{m}^2 \cdot \text{s}^{-1}$ at room temperature. Our membranes are in the gel phase where the dynamics are 1000 times slower than in the fluid phase, but still fast enough to allow small segments of the DNA chain to move and rearrange at the surface. Thus, we can study the influence of the charge density without risks of freezing the conformations. To our knowledge this is the first time that charged lipid membranes have been used to observe supercoiled DNA conformations by AFM. In contrast to bare mica or polylysine films, a membrane is a soft, elastic substrate for the deposition of DNA. It allows the molecule to rearrange. On mica, in the presence of divalent cations, the location of the surface charges is constrained by the crystal lattice. On membranes, charges are fairly mobile. We study the influence of the surface charge density on the conformation of supercoiled DNA. We observe various 2D equilibrium conformations: plectonemic conformations as well as open conformations or loose conformations with only a few crossings. This merely depends on the amount of mobile charges around the molecule, either in the solution or at the surface. We show that in a similar manner to salt in bulk, surface charges screen the phosphate charge on the DNA backbone resulting in an evolution of supercoiled DNA conformations to more regular and more writhed when surface charge is increased. We compare the efficiency of surface screening and bulk screening (from salt), using two sets of experiments.

Materials and methods

AFM

All experiments were performed in tapping mode in a liquid cell of a multimode AFM connected to a nanoscope III controller (Bruker, Santa Barbara). The cantilevers were TAP75 from "Nano and more". The volume of the cell is approximately 400 microliters.

The diluted DNA solution was injected into the AFM fluid cell and allowed to adsorb gently on the membrane. Imaging of the conformation of the DNA took place immediately after the injection. A very gentle force was applied. By using small attenuations of the working amplitude we tend to prevent deformation or degradation of the molecule by the tip.

Substrate preparation

Because of its atomic smoothness, mica was chosen for the bare substrate. However, it is negatively charged, therefore it needs to be modified to promote DNA adhesion. To bridge the macromolecule and the mica, we have chosen charged supported lipid bilayers as a substrate. These model membranes are formed by vesicle fusion on mica⁴⁴. By adjusting the ratio between a positively charged lipid and a neutral phospholipid we can vary the surface charge density. Assuming that the proportion of charged lipids within the bilayer is the same as the one within the starting lipid mixture, we can evaluate quantitatively this surface charge density. Liposomes of 30 nm in diameter on average, as determined by dynamic light scattering, are formed by tip sonication of a solution of a mixture of lipids diluted in pure MilliQ water or buffer. The lipid concentration is (0.24 mg/mL). The two lipids chosen are Di-Palmytoyl-Trimethyl-Amonium-Propane, chloride salt (DPTAP), and Di-Palmytoyl-Phosphatidyl-Choline (DPPC) (Avanti Polar Lipids). They only differ by their head, DPTAP being positively charged, while DPPC is zwitterionic. Their fluid-gel transitions are respectively 41 and 46°C, therefore we heated up the vesicle solution during sonication, 20 °C above the fluid gel transition. The hot solution was injected immediately after sonication into the fluid cell of the AFM. When floppy nano vesicles break on the cold mica, they form instantaneously a bilayer that cools rapidly down. The membrane was rinsed with 3 mL water at RT or buffer with the same salt concentration. The obtained bilayers are in the gel phase. They are particularly smooth, even smoother than the bare substrate because they partially absorb the corrugation of the mica. However, due to the mechanism of formation of the bilayer, i.e. small patches nucleating and growing, grain boundary and sometimes small holes showing the bare mica are clearly visible on the AFM images. Mixed DPPC DPTAP bilayers are homogenous at low DPTAP content. Above 50% of DPTAP, we see the appearance of lipid domains of different heights. The domains size does not evolve with time. In the thinner domains, lipids are tilted. These domains also exist at 100% of DPTAP with a higher thickness

difference. Most of the time, tilted domains are smaller than the size of the macromolecule and the surface present fractal like digitations. Similar domains have been described by Radler and coworkers⁴⁵ for DMPC/DMTAP mixed bilayers. The authors have evidenced a non-linear behaviour of the fluid/gel transition of the lipid mixtures. The temperature T_m , at which the lipids main transition occurs, increases up to 45% of DMTAP before decreasing again. They also performed Langmuir isotherms by compressing monolayers of different mixtures at the air water interface. They have shown that at a fixed high pressure, the area per lipid in the monolayer presents a minimum around stoichiometry 1:1.

They explain these results by the fact that there should be a high affinity between the phosphate group of the PC head and the ammonium group of the TAP, which is maximized for stoichiometry 1:1. From SAXS results, they deduced that at high DMTAP contents, small domains of solid phases of stoichiometry 1:1 would be embedded in a matrix of LC phase. Although bilayers and monolayers can behave differently; we have performed Langmuir isotherms on DPPC/DPTAP mixed monolayers, which shall give us a good insight into the interactions between the two lipids used in this work. We show them in supplementary information. The presence of DPTAP in the monolayer results in the disappearance of the LE/LC plateau of pure DPPC. Increasing the DPTAP content in monolayers, results in a shift of the isotherms to smaller areas. The minimum is achieved at a 50-50 ratio. Above 50 % of DPTAP, the isotherms are shifted back to the large areas. However, the area per lipid head at fixed pressures hardly changed, in contradiction to what was reported for DMTAP/DMPC mixtures by Radler and coworkers. In conclusion, the surface charge density of the mixed DPPC/DPTAP bilayers shall not be much affected by the peculiar phosphate-ammonium affinity. Moreover, all the quantitative analysis that we have pursued in this article, have been performed at low surface charge densities where the bilayers are still homogenous.

DNA

The DNA used for this study is supercoiled pUc19 2686 base pairs long from New England Biolabs (NEB). It was aliquoted as received (1mg/mL in 10mM Tris buffer), without any further purification. This supercoiled DNA appears to be particularly pure of broken or relaxed circles. The manufacturer gives a specification of at least 90% of the DNA in the supercoiled form but agarose gel electrophoresis (1%) performed on several batches in presence of ethidium bromide showed only one bright spot indicating that apparently no relaxed, linear DNA or other sizes of supercoiled DNA were present. One aliquot containing 1 μ g of stock DNA was unfrozen a few minutes before each experiment and diluted in ultra-pure milliQ water (resistivity 18.2 M Ω .cm) or in buffer solutions to reach a final concentration of 1 μ g/mL.

It is commonly assumed that DNA is not stable in pure water at room temperature^{46 47}. But how fast the denaturation takes

place is still an issue. We used the hypochromism of DNA to determine the kinetics of denaturation of pUc19 DNA in the conditions of our AFM experiments⁴⁸. The absorbance of the solution at 260 nm was stable for more than twelve hours at RT. It increased rapidly and reached a plateau when heating the sample up to 80°C (See supplementary information fig. S1). This result clearly shows that the DNA we used is stable enough at RT for the time of our AFM experiment although it denatures quickly at 80°C. This result is not in contradiction with the existence of denaturation bubbles along the chain. However, the fact that plasmids are supercoiled might prevent a complete denaturation at large scale at RT. The precision of the measurement is given by the signal to noise ratio on the UV absorbance signal. It did not seem to evolve with time or be larger than for DNA dissolved in buffer solution.

To assess the exact linking number of our DNA, we performed 1D agarose gel (1.5 % w/w) electrophoresis in presence of chloroquine (2 μ g/mL) at 20V for 17h. Chloroquine is an intercalating agent inducing positive superturns and thus reducing negative supercoiling of DNA. An appropriate concentration allows a separation of the topoisomers (Fig. 1).

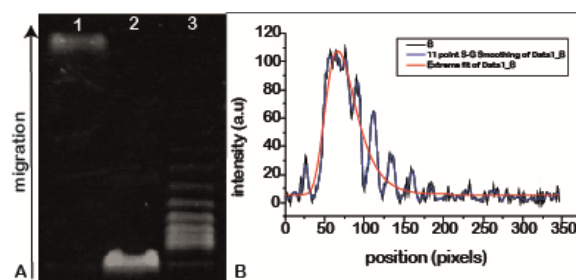


Fig.1 A: Agarose gel electrophoresis (1%) of pUc 19 DNA in presence of chloroquine (2 μ g/mL). Lane 1: Closed circular pUc19 DNA (Relaxed by nicking and re ligated). Lane 2: open circular (one strand nicked) pUc19 DNA (relaxed by nicking). Lane 3: native supercoiled pUc 19 DNA (initially negatively supercoiled). **Fig.1** B: intensity line profile of lane 3.

As a control, we injected at the same time relaxed pUc19 (one strand nicked with NtbspqI (NEB) and relaxed pUc19 that was afterward religated with T4 DNA ligase (NEB). Both restriction and ligation were done following the manufacturer protocol. The DNA was purified using a Miniprep PCR purification kit (Qiagen) and resuspended in 10 mM Tris buffer at pH 7.5 before being run through the gel. The conformation of relaxed supercoiled DNA (one strand nicked) is not modified by the presence of chloroquine. As it is circular, its hydrodynamic radius is large and the migration on the gel is the slowest (lane 2). Relaxed DNA that has been religated is positively supercoiled by chloroquine and migrates the fastest (lane 1). The spot of the native pUc19 appears in between (lane 3). A line profile of lane3 is given on figure 1.B. Fitting the intensities with a skewed Gaussian curve gave on averaged, $\Delta L_k = -7$. This value is in agreement with the literature³⁶.

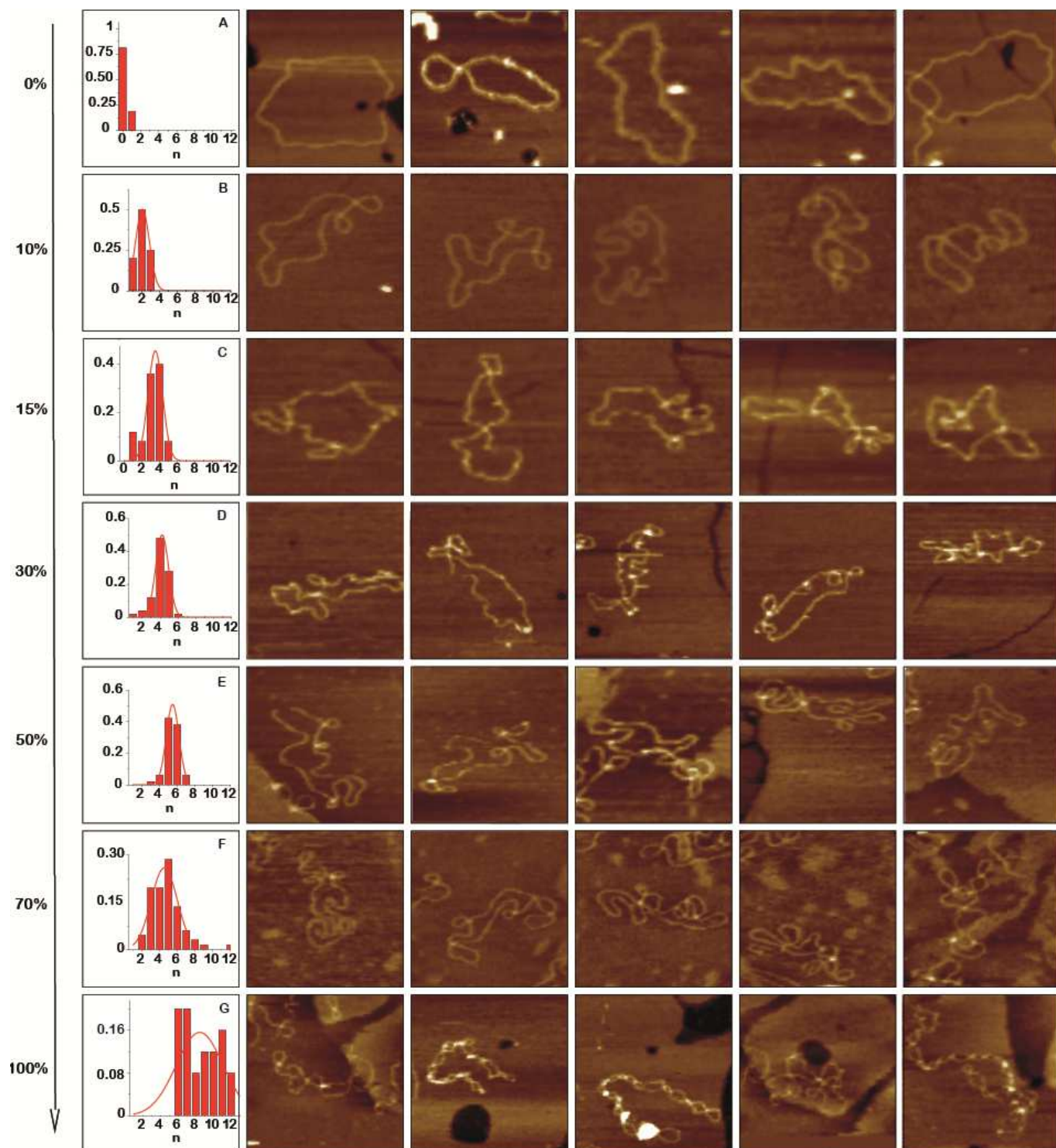


Fig. 2 A to G show 400 x 400 nm zooms of representative pUc19 DNA conformations. Plasmids are diluted in milliQ water and adsorbed on bilayers with a controlled surface charge containing a fraction of cationic lipid of 0, 10, 15, 30, 50, 70 and 100 % respectively. On the left, the corresponding normalized histograms of the number of nodes (number of crossings) with Gaussian fit.

Results and discussions

Deposition of supercoiled DNA from pure water on charged membranes

In a first set of experiments we have studied the conformation of supercoiled pUc19 that we allow to adsorb on lipid bilayers with DPTAP content ranging from 0% to 100%. For the purpose of the experiment we get away from physiological conditions and dilute our DNA in milliQ water.

Working in salt free solution allows us to explore a much larger range of DNA surface interactions. After dilution, the residual salt concentration was 10^{-5} M; as shown in the supplementary materials, in such a dilution our plasmids are stable at RT for more than 10 hours.

Typical conformations of supercoiled pUc19 DNA in milliQ water are shown on Fig. 2 (mixed DPPC/DPTAP bilayers) and Fig 3 (pure DPPC). For each surface charge on Fig. 2, we present a series of zooms on single molecules; all conformations within the population studied look relatively similar, with of course some variations.

Next to the AFM images on Fig. 2, we present normalized histograms of the number of nodes (crossovers between strands) and the corresponding Gaussian fit (red line). For each experiment, the statistic was done on fifty molecules on average. For DPTAP fractions above 50%, the nodes number dispersion is quite large, due to surface inhomogeneities. For the pure DPTAP surface it was rather difficult to count nodes: the superhelix was really tight and the AFM tip had trouble resolving the tertiary structure. Discarding this additional surface complexity, we averaged the number of nodes over the entire surface, but restricted our further data analysis to low surface charge densities where the membrane looks homogenous at nanoscopic scale.

On DPPC (Fig. 2A and 3), Plasmids adopt an open circular conformation in milliQ water. For the record, nicked circles also adopt the same open circular conformation on DPPC. However, plasmids were not nicked in bulk, as shown in the material and method section, and it is unlikely that the adhesion to the substrate would have only broken one strand. In such a geometry pUc19 DNA with a ΔL_k of -7 must be particularly constrained. Besides, the surface of DPPC is neutral (in fact zwitterionic), but we do see DNA adhesion. When approaching the membrane, plasmids should be repelled by their own image charge, which is due to the high dielectric contrast between the membrane and water. Therefore there must be some kind of compensating short range interaction that allows for adhesion. The origin of this short range attraction is unclear but we speculate a dipole-charge interaction, the positive charge of the dipole being pointing out of the membrane.

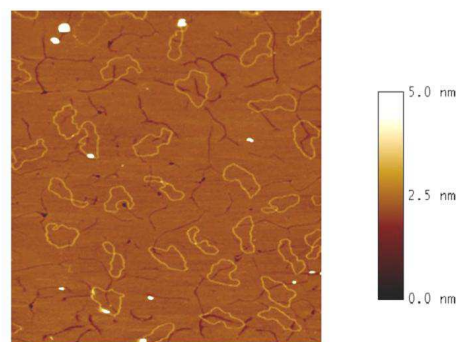


Fig.3 AFM image ($5\mu\text{m} \times 5\mu\text{m}$) of pUc19 plasmids adsorbed on DPPC in salt free solution. Most of the conformations are open rings although the DNA is not nicked. A small fraction of plasmids over cross strands in a perpendicular manner.

On DPPC-DPTAP mixed bilayers, as seen on Fig 2B to 2G, writhing increases with surface charge fraction. For low surface charges, plasmids adopt relatively loose conformations, which tighten along with an increase of the surface charge density. We have noticed that plasmid shapes vary slowly, with nodes shifting along the closed chain, presumably to reach the most stable conformation in 2D. At equilibrium, supercoiled DNA molecules end up in conformations with small loops scattered along a main cycle. Hence, if the crossings are well scattered all over the DNA molecule just after immobilization, their positions evolve during the first minutes. After some time, there is equilibrium of very small loops next to much larger ones. This effect has been previously reported in the literature, in computer simulations performed on 2D knots^{49, 50}. When charges are added to the bilayer, the superhelix writhes more and more until it reaches the plectonemic conformation that was so often reported in the literature.

Additionally, as one can see on Fig. 4, relaxed pUc19 DNA is insensitive to surface charge as it stays perfectly open on 50% DPTAP surface.

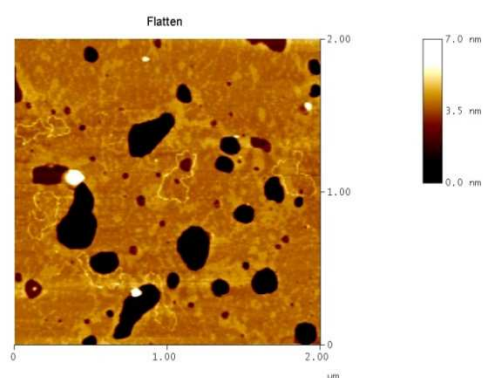


Fig.4 Open circular (one strand nicked) pUc19 DNA adsorbed on a 50% charged membrane. The DNA is lying open on the surface. There is no apparent crossing of strands in the tertiary structure. Black areas are holes in the bilayer that let appear the mica substrate underneath.

All surface interactions are likely to be similar for nicked circular DNAs and for closed constrained circular DNAs. We thus deduce that for wild (non-nicked) plasmids, the additional internal stress due to extra turns is accountable for writhing and that supercoiling is made easier and easier when the surface charge is increased.

This writhing along with a surface charge increase can be explained with the help of a simple physical argument.

Indeed, in a recent analytical study⁵¹ we show that in salt free solution, for constrained polyelectrolytes adsorbed in 2D, the electrostatic interaction at crossing is dominant compared to other interactions. When charges are added to the bilayer, the polarizable interfacial charge screens the DNA charges and thus reduces the electrostatic repulsion at crossings.

On DPPC, the zwitterionic surface, the membrane is neutral. DNA bears counter-ions which ordinarily reduce its internal charge. The electrostatic energy needed for crossing strands in 2D is of the order of one hundred of $k_B T$, it exceeds bending and twisting costs (tenths of $k_B T$). Therefore, a DNA molecule would prefer to be under high twist rather than having crossings. Rings are more favourable than conformations with one single crossing (“figures of eight”), even though DNA is highly constrained.

For charged surface, DNA plasmids do feel the surface potential. The repulsion between strands is reduced; twist might be partially traded against writhe.

For moderate surface charge densities, we experimentally noticed that crossovers are right-angled. This is strong evidence that electrostatic repulsion at crossings is dominant. On highly-charged surfaces however, we observe plectonemes. The angle at crossings is of the order of 30° . Introducing an extra superhelical turn is more favourable than having torsion within the chain.

More precise consideration of electrostatics effects shows indeed that the surface charges provide some screening and play a similar role to ionic charges in solution. In order to get a better picture of the problem, we need to introduce a few concepts.

At surface carrying μ charges per unit area, DNA chains adopt a flat conformation and are confined within a counter-ion layer whose thickness is characterized by the so-called Gouy-Chapman (GC) length λ from the surface.^{52, 53}

The effective charge of the plasmid is fixed by the interplay between electrostatic interactions and entropy. In solution, it is rather simple; cations condense on the negatively charged backbone of the plasmids. This counter-ion layer reduces significantly the repulsive electrostatic interaction between charged phosphate groups of DNA chains.

On positively charged surfaces, the vicinity of the surface further reduces the electrostatic interaction between DNA charges. Because of the annealed surface charges, since mobile surface charges tend to accumulate under the DNA (Fig. 5), this additional screening is somewhat stronger. At the same time,

the electrostatic potential of the surface repels cations condensed on the plasmid. They will be released to a large extent, which will drastically increase their entropy. As a result, the final net charge of the plasmid (condensed cations + DNA) shall be larger than for a plasmid only subjected to counter-ion condensation in solution.^{51, 54}

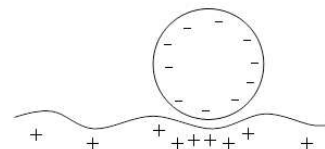


Fig.5 Sketch of a charged rod adsorbed on an oppositely charged membrane with mobile charges. Drawing bulk counter-ions has been voluntary omitted.

Comparison of conformations with charges at the surface or in volume

To compare the effect of surface charges with the effect of charges in bulk, we have performed a second set of experiments on the zwitterionic DPPC surface with addition of salt in solution. This set of experiments showed, as expected, supercoiled conformations with an increase of the number of nodes when the salt concentration was increased. We present typical conformations in Fig. 6A to 6E, accompanied by histograms of the node numbers (Fig. 6F-J). As already shown by others in the literature, the conformation of supercoiled DNA shows more writhe as the salt concentration of the solution is increased. Adhesion to the substrate was rather weak above 10 mM of salt. Hence, plasmids appeared to be whitish on the image Fig. 6D and 6E, indicating that they were almost not touching the substrate. We encountered a lot of trouble imaging at 30mM therefore the node number was not counted (Fig. 6J).

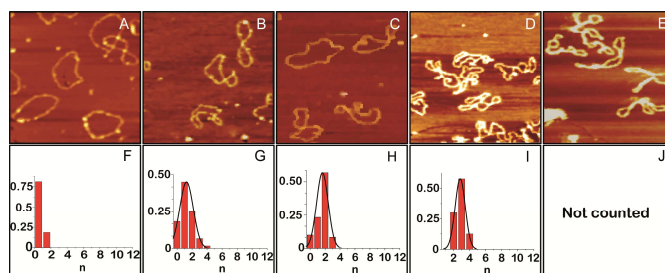


Fig.6 Effect of salt addition on the adsorption of plasmid DNA onto an uncharged DPPC bilayer. From A to E: $1\mu\text{m} \times 1\mu\text{m}$ AFM zooms showing the effect of increasing salt concentration, respectively 0, 1, 5, 10 and 30 mM of NaCl. From F to J: the corresponding statistical analysis of the number of nodes. The number of DNA superturns increases along with the bulk salt concentration, but at the same time the affinity for the surface is reduced and imaging becomes very difficult. The colour scale is the same as on Fig.3.

From the two sets of experiments that we have performed we can compare the screening effect from charges at the surface and from charges in bulk.

We expect to see similar behaviour for surface screening and bulk screening.

For a charged object in solution in the vicinity of a membrane, the electrostatic potentials involved are namely the GC potentials V_{GC} for surface screening and the Debye-Hückel (DH) potential V_{DH} for bulk screening. Both potentials are characterized by a single screening length; respectively the GC length λ and the Debye length κ^{-1} .

The number of nodes n being a direct indicator of the screening efficiency, we plot it as a function of both screening lengths.

$$\lambda = \frac{e}{2\pi \cdot l_B \cdot \mu}$$

$\kappa^{-2} = 8\pi l_B C_s$ with C_s the bulk monovalent salt concentration and l_B the Bjerrum length.

$$l_B = \frac{e^2}{4\pi\epsilon_0\epsilon_r k_B T}$$

κ^{-1} is of the same order of magnitude than λ ⁵⁵. However the two potentials (GC and DH) do not have the same dependence with their respective screening length, therefore we will only retain that $\kappa^{-1} \propto \lambda$ without any pre estimation of the coefficient of proportionality.

In order to get λ , one needs beforehand to compute the surface charge density of the bilayers μ . In the moderate screening regime, this surface charge density is proportional to the fraction of cationic lipids within the bilayer f , and inversely proportional to the mean area per lipid head in the bilayer $A_{bilayer}$.

$$\mu \propto \frac{f}{A_{bilayer}}$$

For highly charged surfaces this would not be the case any longer. There would be a greater ionic organization within the GC layer. Counter-ions condensation could also take place until the effective distance between charges matches l_B . We did not take this effect into account in our calculation and use only nominal values of μ .

While a surface per lipid head of 64 \AA^2 is commonly admitted for a DPPC bilayer as measured by neutron reflectivity⁵⁶, for pure DPTAP and all DPPC/DPTAP mixed bilayers, we have not found any data in the literature. We expect similar behaviour for monolayers and bilayers; therefore we will evaluate the area per lipid head in the bilayer by using the data measured in the monolayer. As specified before (see material and methods), for mixed DPPC-DPTAP monolayers, the mean area per lipid head undergoes non-linear but small variations of less than 10% depending on the DPTAP content. Nonetheless, it is not easy to estimate what would be the area per lipid head in the bilayer. Transfers are usually performed around 30

mN/m. Although for DPPC where both values of the area per molecule are known, the area of the monolayer at this pressure does not correspond to the one of the bilayer. Assuming that the area variation relative to the DPTAP composition is the same within the bilayer than within the monolayer, we estimated the area per lipid in the mixed bilayers. We compared the areas obtained for mixed DPPC-DPTAP monolayers with the pure DPPC monolayers and transposed the variations to bilayers of the same compositions. The surface charge density with respect to the DPTAP proportion was subsequently computed. Results are presented in Table 1.

Table 1 Area per lipid head for pure and mixed monolayers of DPPC /DPTAP measured at 30mN/m. Estimation of the corresponding area in the bilayer of the same composition as compared to pure DPPC where the area in the bilayer was previously measured by Neutron reflectivity. Corresponding computed surface charge density of the bilayer and estimation of the distance between charges. Bold values are measured

% DPTAP	$A_{\text{mono}} (\text{\AA}^2)$	$A_{\text{bilayer}} (\text{\AA}^2)$	$\mu (e \cdot \text{\AA}^{-2})$	$d_{\text{charges}} (\text{\AA})$
0	43	64 (a)	0	
10	41	62.7	0.0016	25
15	40	62.4	0.0025	20
30	40	62	0.0048	14
50	40	62.08	0.0081	11
70	42	63.3	0.0111	9.5
100	43	64	0.0156	8

a. As measured in ref⁵⁶

The resulting node numbers as a function of the screening lengths are presented on Fig. 7

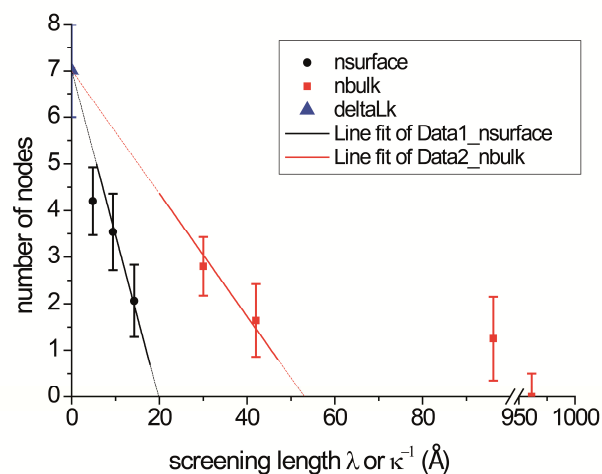


Fig.7 Comparison of the efficiency of surface screening and bulk screening. We measured the crossing number as a function of the corresponding screening length in the case of the Gouy-Chapman (black solid circles) and Debye Huckel (red solid squares) theories respectively. As predicted by the analytical model of ref 51, the extrapolation at zero screening length of the mean field regime shall be ΔL_k . We plotted the value measured by electrophoresis (blue triangle).

For both types of screening, we see that the number of nodes decreases with the screening length. It drops to zero for large screening lengths.

We will use the results of ref ⁵¹ to analyse our data. This analytical model was developed in the mean field approach.

For a plasmid adsorbed in 2D at the surface, the minimization of the total free energy of the plasmids with respect to n shows that the free energy has a linear dependence on n .

$$|n| = -\frac{L}{4\pi^2 l_t} (F_h + F_{cross}) + |\Delta L_k|$$

with L is the contour length of the plasmid, l_t is the twist length, F_h the free energy of interaction with the surface and F_{cross} is the penalty for crossing helices in 2D. F_h can usually be neglected in front of F_{cross} . n and ΔL_k are negative by definition for a plasmid negatively supercoiled. A linear dependence with λ or κ^{-1} is hidden in F_{cross} .

Writhing is thus only a question of how we screen the electrostatic penalty for crossing helices in 2D.

The minimum of electrostatic free energy is obtained when the segments are perpendicular to each other as we also witnessed in the experiments for moderate range of screening. We only consider this case in the following:

$F_{cross} = \tilde{V}(q=0)$ where $\tilde{V}(q=0)$ is the FT of the potential taken at the surface.

$\tilde{V}_{GC}(q=0) = \frac{4}{3} \pi l_B \rho_\lambda^2 \lambda$ with ρ_λ the linear charge density of DNA in the case of surface screening. The above formula takes into account the fact that in the presence of annealed charges, the GC potential is reduced by a factor of 3 due to lipids mobility.

$$\tilde{V}_{DH}(q=0) = 2\pi l_B \kappa^{-1} \rho_\kappa^2$$

with ρ_κ the linear charge density of DNA for bulk screening. For both types of screening, the intercept of the line should give $|\Delta L_k|$. As we only have a few data points, in order to minimize the error on the slopes, we used the value of $|\Delta L_k|$ which was independently measured as a starting point of our fits. This data point should be common for surface and bulk screening if one only considers the electrostatic cost. This point at zero screening lengths is only an extrapolation of the mean field regime. For highly charged surfaces, and high salt concentrations, other types of interactions do play a role (for instance bending).

For surface screening we use only the data points in a moderate range of screening, i.e. where the coupling between counter-ions is weak.

In practice, the limit occurs between the data points at 15 % ($\lambda=9.45 \text{ \AA}$) and 30 % of DPTAP ($\lambda=4.69 \text{ \AA}$). We plotted the value at 30 % as well as it helps to see a trend.

From the all set of data, we only have two points that surely belong to the mean field regime: the points at 10% and 15% of DPTAP. Using, these points, we find a line with a slope $S_\lambda=0.35 \text{ \AA}^{-1}$. As expected the data point at 30% DPTAP slightly deviates from the mean field regime. The linear dependence is also cut at low number of nodes when the curve must smoothly goes to zero.

From the slope, we can deduce the linear charge density of the plasmid when adsorbed on charged surfaces. We found a value of $1.5 e^-$ per Bjerrum length, which is the effective linear charge density of the plasmid including its cloud of counter-ions. It has been increased by one third as compared to what is usually assumed in salty bulk solutions. This is consistent with the fact that some counter-ions have been released during adsorption.

For bulk screening, the number of nodes is also decreasing but less sharply. At large screening length it is nevertheless null. The linear dependence must only be valid for moderate screening lengths, therefore we discarded the points at $\kappa^{-1}=96$ and $\kappa^{-1}=960 \text{ \AA}$.

The straight line based on the first three data points has for slope $S_\kappa=0.13 \text{ \AA}^{-1}$.

By comparing the slopes S_κ and S_λ , one obtains the ratio:

$$\frac{S_\lambda}{S_\kappa} = 2.67$$

For a specific node number n , the two DNA segments at crossing must be screened the same way by a DH or by a GC potential, the value of the two interactions (penalty for crossing helices) are thus equal. This suggests that the ratio of effective charges is

$$\frac{2}{3} \rho_\lambda^2 / \rho_\kappa^2 = 2.67 \text{ and then } \frac{\rho_\lambda}{\rho_\kappa} = 2$$

The linear charge density of DNA appears to be two times smaller for bulk screening than for surface screening, which is compatible with our assumption that DNA has less condensed counter-ions on charged surfaces than in bulk. On DPPC, this gives approximately a DNA effective linear charge density of $0.75 e^-$ per l_B which is smaller than what is usually assumed for DNA in salt solutions. It is compatible with the idea that, in order to compensate for the repulsion of plasmids by their own image charge, there is over-condensation of counter-ions, which further reduces the effective linear charge of DNA.

On the neutral bilayer (zwitterionic), counter-ion condensation is slightly enhanced while on the charged bilayer, there is counter-ion release.

Hence, we experimentally demonstrated that screening from charges at the surface is equivalent to screening from salt in

bulk solution. It is only a matter of how many mobile charges are available around the crossing.

At large Debye screening lengths, i.e. at $\kappa^{-1}=96\text{\AA}$ and $\kappa^{-1}=960\text{\AA}$, the analytical model shows huge electrostatic repulsion, (at this distance the electrostatic cost for crossing helices in 2D is above $100 k_{\text{B}}T$ ^{19,57}), however, experimentally the distribution of nodes was non-zero. The occurrence of one crossing conformations (“figure of eight”) and two crossings was of the order of 20% of the overall plasmid population for $\kappa^{-1}=960\text{\AA}$ and above 60% for $\kappa^{-1}=96\text{\AA}$, which is extremely large considering the energy cost given by the model. We shall expect that counter-ions condensation would have taken place at the crossover, which shall decrease the effective energy cost, but it would not be sufficient to decrease it by one order of magnitude. We postulate that for these two data points, the conformations we have imaged are not fully 2D equilibrated as the model presupposed. Loose writhe might be possible in 3D although in 2D it is energetically not favourable. DNA molecules enduring a rapid transition between 3D and 2D might sometimes trap some writhe during adsorption. We compare it to 3D freezing.

This could be the result of a side effect that occurs during the adsorption step. We guess that it has something to do with the existence of a repelling image charge. Plasmids shall stand perpendicular to the surface before adhering, which will increase the probability of forming writhe.

This presumed additional “frozen crossing” might shift the average node number by one, but it cannot account for more than one. In this case, distributions shall look slightly asymmetric, which seems indeed to be the case at $\kappa^{-1}=96\text{\AA}$. When salt is added to the bulk, the repulsion between the plasmid and its image charge is decreased and the proportion of this extra node to the overall population of nodes must be less. The average node number shall then be more reliable. For charged surfaces, this problem does not exist. Plasmids must already feel the surface potential and stand parallel to the surface before adhering. They have time to equilibrate. Considering that we have a few numbers of data points available in the valid range of screening lengths where the analytical model does apply, our estimation of the effective charge density of DNA when adsorbed at an interface shall then be truthful, but with a rather large error bare.

Conclusion:

In this article we have presented experiments realized on pUc19 plasmid DNA adsorbed on a bilayer and changed the surface charge density to see its effect on the 2D supercoiled conformation of the DNA. We have been able to reproduce many conformations reported in literature either by AFM or by TEM, just by changing the surface charge. In pure water, the most important energetic cost is the repulsion at crossing which cannot be avoided in 2D. In the absence of electrostatic screening, in bulk or at the surface, the molecule favours open

circular conformations, even though it remains very constrained by the linking number. When charges are added at the surface, the mobile lipids reduce the effective charge of the DNA backbone, and supercoiling occurs. It is non-trivial, that the stronger interaction could favour nodes formation. Naively, one would think instead that a greater affinity between plasmids and surface would untighten them. By demonstrating experimentally the equivalence of surface screening and bulk screening we show that electrostatic screening dominates. The presence of mobile charges at the surface does play a very important role. The mobility of the lipids ensures the 2D equilibrium of the molecule but it enhances surface screening as well. As a direct consequence of different counter-ions condensation mechanisms, the effective charge density of plasmids appears to be larger for surface screening than for bulk screening.

As a general rule, membranes of other lipid compositions can also be a good substrate to study the dynamics of macromolecules or macromolecules at 2D equilibrium⁵⁸. The similar case of interaction between anionic lipids and cationic biomolecules is also of interest. In the present case, the DNA is negatively charged and the membrane underneath is positively charged. In protein- membrane interactions, both charges are of reversed sign. Cell membranes are negative and objects that bind to them are positive. Nevertheless, electrostatic effects would lead to similar consequences.

Acknowledgments

The authors thank Albert Johner for fruitful discussions and critical corrections of the manuscript.

References

1. R. Dulbecco and M. Vogt, *Proceedings of the National Academy of Sciences*, 1963, **50**, 236-243.
2. N. R. Cozzarelli, *Science*, 1980, **207**, 953-960.
3. S. A. Wasserman and N. R. Cozzarelli, *Science*, 1986, **232**, 951-960.
4. A. Kornberg, *Journal of Biological Chemistry*, 1988, **263**, 1-4.
5. L. Postow, N. J. Crisona, B. J. Peter, C. D. Hardy and N. R. Cozzarelli, *Proceedings of the National Academy of Sciences of the United States of America*, 2001, **98**, 8219-8226.
6. M. Gellert, *Annual Review of Biochemistry*, 1981, **50**, 879-910.
7. D. S. Horowitz and J. C. Wang, *Journal of Molecular Biology*, 1984, **173**, 75.
8. G. Witz and A. Stasiak, *Nucleic Acids Research*, 2010, **38**, 2119-2133.
9. F. H. Crick, *Proceedings of the National Academy of Sciences*, 1976, **73**, 2639-2643.
10. T. C. Boles, J. H. White and N. R. Cozzarelli, *Journal of Molecular Biology*, 1990, **213**, 931.
11. J. C. Wang, *Journal of Molecular Biology*, 1974, **87**, 797.
12. D. E. Depew and J. C. Wang, *Proceedings of the National Academy of Sciences*, 1975, **72**, 4275-4279.
13. P. Anderson and W. Bauer, *Biochemistry*, 1978, **17**, 594.

-
14. M. Adrian, B. ten Heggeler-Bordier, W. Wahli, A. Z. Stasiak, a. Stasiak and J. Dubochet, *The EMBO journal*, 1990, **9**, 4551.
 15. J. M. Sperrazza, J. C. Register Iii and J. Griffith, *Gene*, 1984, **31**, 17.
 16. C. Brack, *CRC critical reviews in biochemistry*, 1981, 113.
 17. J. Bednar, P. Furrer, A. Stasiak, J. Dubochet, E. H. Egelman and A. D. Bates, *Journal of Molecular Biology*, 1994, **235**, 825.
 18. A. V. Vologodskii and N. R. Cozzarelli, *Annual Review of Biophysics and Biomolecular Structure*, 1994, **23**, 609-643.
 19. T. Schlick, B. Li and W. K. Olson, *Biophysical journal*, 1994, **67**, 2146.
 20. J. Langowski, U. Kapp, K. Klenin and A. Vologodskii, *Biopolymers*, 1994, **34**, 639.
 21. J. A. Gebe and J. M. Schurr, *Biopolymers*, 1996, **38**, 493.
 22. V. V. Rybenkov, A. V. Vologodskii and N. R. Cozzarelli, *Journal of Molecular Biology*, 1997, **267**, 299.
 23. V. V. Rybenkov, A. V. Vologodskii and N. R. Cozzarelli, *Journal of Molecular Biology*, 1997, **267**, 312.
 24. S. Mehmet and et al., *Physical Review E*, 2010, **81**, 041916.
 25. C. Bustamante, J. Vesenka, C. L. Tang, W. Rees, M. Guthold and R. Keller, *Biochemistry*, 1992, **31**, 22.
 26. A. Schaper, J. P. Starink and T. M. Jovin, *FEBS Lett*, 1994, **355**, 91.
 27. B. Samori, G. Siligardi, C. Quagliarello, A. L. Weisenhorn, J. Vesenka and C. J. Bustamante, *Proceedings of the National Academy of Sciences*, 1993, **90**, 3598-3601.
 28. M. Bezanilla, S. Manne, D. E. Laney, Y. L. Lyubchenko and H. G. Hansma, *Langmuir*, 1995, **11**, 655.
 29. Y. L. Lyubchenko and L. S. Shlyakhtenko, *Proceedings of the National Academy of Sciences*, 1997, **94**, 496-501.
 30. K. Rippe, N. MÄycke and J. r. Langowski, *Nucleic Acids Research*, 1997, **25**, 1736-1744.
 31. M. Tanigawa and T. Okada, *Analytica Chimica Acta*, 1998, **365**, 19.
 32. G. Zuccheri, R. T. Dame, M. Aquila, I. Muzzalupo and B. Samori, *Applied Physics A: Materials Science & Processing*, 1998, **66**, S585.
 33. M. Bussiek, N. Mucke and J. Langowski, *Nucleic Acids Research*, 2003, **31**, e137.
 34. J. Fogg, M. and et al., *Journal of Physics: Condensed Matter*, 2006, **18**, S145.
 35. D. J. Billingsley, J. Kirkham, W. A. Bonass and N. H. Thomson, *Physical Chemistry Chemical Physics*, 2010, **12**, 14727.
 36. S. S. Zakharova, W. Jesse, C. Backendorf, S. U. Egelhaaf, A. Lapp and J. R. C. van der Maarel, *Biophysical journal*, 2002, **83**, 1106.
 37. J. Dubochet, M. Adrian, J.-J. Chang, J.-C. Homo, J. Lepault, A. W. McDowall and P. Schultz, *Quarterly Reviews of Biophysics*, 1988, **21**, 129-228.
 38. J. A. Gebe, J. J. Delrow, P. J. Heath, B. S. Fujimoto, D. W. Stewart and J. M. Schurr, *Journal of Molecular Biology*, 1996, **262**, 105.
 39. A. V. Vologodskii, S. D. Levene, K. V. Klenin, M. Frank-Kamenetskii and N. R. Cozzarelli, *Journal of Molecular Biology*, 1992, **227**, 1224.
 40. Y. S. Velichko, K. Yoshikawa and A. R. Khokhlov, *Biomacromolecules*, 2000, **1**, 459.
 41. B. S. Fujimoto and J. M. Schurr, *Biophysical Journal*, 2002, **82**, 944.
 42. C. Rivetti, M. Guthold and C. Bustamante, *Journal of Molecular Biology*, 1996, **264**, 919.
 43. C. Scomparin, S. Lecuyer, M. Ferreira, T. Charitat and B. Tinland, *Eur. Phys. J. E*, 2009, **28**, 211-220.
 44. R. Richter, A. Mukhopadhyay and A. Brisson, *Biophysical journal*, 2003, **85**, 3035.
 45. R. Zantl, L. Baicu, F. Artzner, I. Sprenger, G. Rapp and J. O. RÄdler, *The Journal of Physical Chemistry B*, 1999, **103**, 10300.
 46. R. J. Owen, L. R. Hill and S. P. Lapage, *Biopolymers*, 1969, **7**, 503.
 47. M. D. Frank-Kamenetskii, *Biopolymers*, 1971, **10**, 2623.
 48. D. Voet, W. B. Gratzer, R. A. Cox and P. Doty, *Biopolymers*, 1963, **1**, 193.
 49. R. Metzler, A. Hanke, P. G. Dommersnes, Y. Kantor and M. Kardar, *Physical Review Letters*, 2002, **88**, 188101.
 50. M. Kardar, *Eur. Phys. J. B*, 2008, **64**, 519-523.
 51. N. K. Lee, T. Schmatko, P. Muller, M. Maaloum and A. Johner, *Physical Review E*, 2012, **85**, 051804.
 52. A. W. Adamson, *Physical Chemistry of Surfaces*, John Wiley and Sons Inc, New York, 1990.
 53. D. Andelman, in *Structure and Dynamics of Membranes*, eds. R. Lipowsky and E. Sackmann, Elsevier Science B.V., North Holland, 1995, vol. 1.
 54. C. C. Fleck and R. R. Netz, *The European Physical Journal E: Soft Matter and Biological Physics*, 2007, **22**, 261.
 55. O. V. Borisov, E. B. Zhulina and T. M. Birshtein, *J. Phys. II France*, 1994, **4**, 913-929.
 56. J. F. Nagle, R. Zhang, S. Tristram-Nagle, W. Sun, H. I. Petrache and R. M. Suter, *Biophysical journal*, 1996, **70**, 1419.
 57. G. L. Randall, B. M. Pettitt, G. R. Buck and E. L. Zechiedrich, *Journal of Physics: Condensed Matter*, 2006, **18**, S173.
 58. T. Heimburg, B. Angerstein and D. Marsh, *Biophysical Journal*, 1999, **76**, 2575.
-